# Improved forward calculation for phase artifacts removal in susceptibility mapping

**S. Liu[1], J. Neelavalli[2], W. Zheng[3], and E. M. Haacke[2,4]**
[1]School of Biomedical Engineering, McMaster University, Hamilton, Ontario, Canada, [2]The Magnetic Resonance Imaging Institute for Biomedical Research, Detroit, Michigan, United States, [3]Biomedical Engineering, Wayne State University, Detroit, Michigan, United States, [4]Academic Radiology, Wayne State University, Detroit, Michigan, United States

**Introduction:** Susceptibility mapping aims to calculate the source of the local field by extracting information from phase images [1]. Thus, relatively pristine phase images containing only phase from inter-tissue susceptibility differences are required for accurate susceptibility quantification. Unfortunately, phase images contain additional artifacts from background field inhomogenieties as well from sources like, eddy currents, shimming etc. While it is common to apply the homodyne high-pass filter (HP) in Susceptibility Weighted Imaging (SWI) to remove low spatial frequency background phase artifacts, HP filtering leads to loss of phase information [2] which adversely affects susceptibility quantification accuracy. Consequently, it is preferable to use a weaker high-pass filter or even completely avoid high-pass filtering when possible. To this end, the forward field calculation, which is based on the relationship between susceptibility distribution and magnetic field variation in Fourier domain, is a very promising solution [3]. Yet sometimes this forward calculation is not sufficient when other phase artifacts sources, such as eddy currents are considerable, for example in multi-echo sequences or segmented k-space acquisitions. To further reduce these remnant phase artifacts, an improved forward calculation method is proposed in this study.

**Materials and Methods:** The forward calculation is based on the relation $B_0 \cdot FT(\chi(r)) \cdot FT(G(r)) = FT(\Delta B(r))$, where $B_0$ is the main magnetic field, $\chi(r)$ is the susceptibility distribution, G(r) is the Green's function, and $\Delta B(r)$ is the induced magnetic field variation. Once the geometry of the object is obtained, the $\chi(r)$ can be determined with a least squares fit and $\Delta B(r)$ can be subsequently calculated. This method, however, does not account for other sources of background field variations such as eddy currents which are commonly present. Since the eddy currents induced phase artifacts, typically present in the read-out direction but may also be present in phase encoding and slice directions depending on how the slice is prescribed, we propose to include additional coefficients for polynomial fitting in the least squares formulation. We tested this method on a dataset for cadaver brain containing large iron content in the basal ganglia. The phantom was prepared by laying the cadaver brain in a rectangular container filled with agarose gel. It was imaged with an 11-echo SWI sequence at 3T, with TR 40ms, BW 465Hz/Pixel, voxel size 0.5x0.5x0.7$m^3$ and matrix size 512x384x40. Strong eddy current effects were seen between the even and odd echoes. Only the datasets from the first two echo times were used in this study, with the first TE=5.68ms, and the second TE = 8.25ms. The phase images from the first TE were complex divided into the phase images at second TE, to generate phase image with an effective TE of 2.57ms. This complex divided phase was first unwrapped and then used to test the effectiveness of different fitting methods. Specifically, first only the forward field calculation was performed. Next, first the linear term and then the quadratic fitting terms were added to the forward calculation. Depending on which method provided best fit for the background phase, the same was applied to unwrapped phase from TE5.68ms. This was done to obtain better phase-SNR from the longer echo data for better susceptibility quantification. Any remnant phase variation after subtraction of predicted phase was filtered using 1) a 16x16, 2) a 8x8 high-pass filter and 3) no high-pass filter. Susceptibility maps were generated using these phase images following the method described in [2].

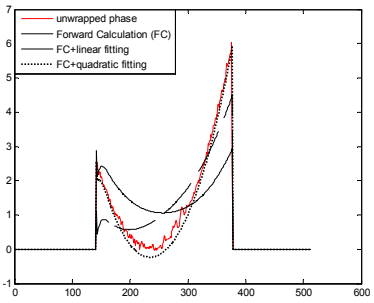


***Figure 1**. Phase profiles along the read-out direction in the unwrapped phase (red line), the phase predicted purely with forward calculation (dark solid line), and the phase predicted by adding linear or quadratic fitting to the forward calculation.*

**Results and Discussions:** As shown in this **Figure 1**, when only the common forward calculation (denoted by "forward calculation" in Figure 1) was used, the predicted phase profile failed to fit the original unwrapped phase profile properly. However, when a quadratic polynomial fitting was added to the forward calculation, relatively satisfying results were obtained. Thus, to minimize remnant phase artifacts, a quadratic fitting was decided upon as necessary for this imaging sequence to remove non-geometry related background field affects. Hence the same method was applied to the TE 5.68ms phase dataset. **Figure 2A, B** and **C** compare the original phase, the phase image obtained after correction using forward field calculation only and the phase image obtained after correction using forward filed estimation and quadratic fitting. After this phase artifacts removal process, relatively pristine phase images were obtained. Some remnant low spatial frequency variations were removed by a mild high-pass filter. While 16x16 high-pass filters were used in **Figure 2.D** and **2.E**, only a 8x8 high-pass filter was used in **Figure 2.F**, which still gives us acceptable quality in the susceptibility map. Comparing **Figure 2.D** with **2.E**, the improvement in susceptibility maps is evident. However, when no high-pass filter is used, as shown in 2.G, the quality of the susceptibility map on the left end is not satisfying. This may be caused by the bias in the fitting of the phase profile in the left-to-right direction.

Susceptibility were measured from different susceptibility maps and compared with each other. Generally, the smaller the high-pass filter size, the less under-estimation we will obtain.

***Table 1. Susceptibility measured for the globus pallidus from different susceptibility maps***

| Fitting method | Forward calculation with quadratic fit | | | Forward Calculation only |
|---|---|---|---|---|
| High-pass filter size | 16x16 | 8x8 | No high-pass filtering | 16x16 |
| Susceptibility(Mean/Std.)/ppm | 0.248/0.081 | 0.276/0.076 | 0.482/0.073 | 0.154/0.086 |

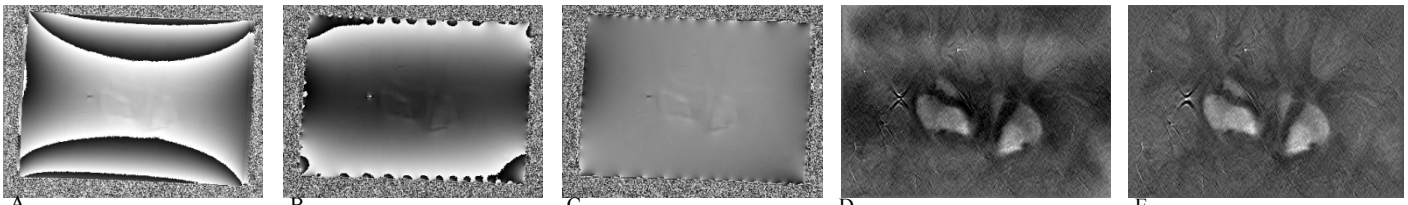


***Figure 2. 2.A** the original phase image. **2.B** phase image after traditional forward calculation **2.C** phase image after forward calculation with a quadratic polynomial fitting in the read-out direction. **2.D** Susceptibility map generated with phase images shown in **2.B**, using a **16x16** high-pass filter. **2.E** to **2.G** are susceptibility maps generated with phase images shown in **2.C**. And a **16x16** high-pass filter was used to generate **2.E**, while a **8x8** high-pass filter was used in **2.F**. No high-pass filter was used in **2.G**. (**2.D** to **2.G** were cropped from the original images and zoomed for displaying.)*

**Conclusion:** With this improved forward calculation, most of the background field variation can be properly predicted and removed. This allows us to use high-pass filters with smaller size to reduce error in susceptibility mapping.

**References:** [1]Haacke et al., MRM, 52:612, 2004 [2] Haacke et al. JMRI(2010) 32:663-676 [3] Neelavalli et al., JMRI(2009);29:938-48